

## Dosimetric characterization and organ dose assessment in digital breast tomosynthesis: Measurements and Monte Carlo simulations using voxel phantoms

Mariana Baptista, Salvatore Di Maria, Sílvia Barros, Catarina Figueira, Marta Sarmento, Lurdes Orvalho, and Pedro Vaz

Citation: *Medical Physics* **42**, 3788 (2015); doi: 10.1118/1.4921362

View online: <http://dx.doi.org/10.1118/1.4921362>

View Table of Contents: <http://scitation.aip.org/content/aapm/journal/medphys/42/7?ver=pdfcov>

Published by the [American Association of Physicists in Medicine](#)

---

### Articles you may be interested in

[Monte Carlo performance on the x-ray converter thickness in digital mammography using software breast models](#)

*Med. Phys.* **39**, 6638 (2012); 10.1118/1.4757919

[Organ doses for reference adult male and female undergoing computed tomography estimated by Monte Carlo simulations](#)

*Med. Phys.* **38**, 1196 (2011); 10.1118/1.3544658

[Comparison of organ doses for patients undergoing balloon brachytherapy of the breast with HDR I 192 r or electronic sources using Monte Carlo simulations in a heterogeneous human phantoma\)](#)

*Med. Phys.* **37**, 662 (2010); 10.1118/1.3292292

[Variations of lung density and geometry on inhomogeneity correction algorithms: A Monte Carlo dosimetric evaluation](#)

*Med. Phys.* **36**, 3619 (2009); 10.1118/1.3168966

[Monte Carlo simulations of dose from microCT imaging procedures in a realistic mouse phantom](#)

*Med. Phys.* **33**, 216 (2006); 10.1118/1.2148333

---



## AUTOMATE YOUR MACHINE QA

### SNC Machine™

- TG-142 & VMAT Test Libraries
- Automated QA File Capture & Analysis
- Works with Varian, Elekta, Aria®, MOSAIQ®

Learn More 

# Dosimetric characterization and organ dose assessment in digital breast tomosynthesis: Measurements and Monte Carlo simulations using voxel phantoms

Mariana Baptista,<sup>a)</sup> Salvatore Di Maria, and Sílvia Barros

*Centro de Ciências e Tecnologias Nucleares, Instituto Superior Técnico, Universidade de Lisboa, Estrada Nacional 10, km 139,7, Bobadela LRS 2695-066, Portugal*

Catarina Figueira

*Centre for Plasma Physics, School of Mathematics and Physics, Queen's University, Belfast BT7 1NN, United Kingdom*

Marta Sarmento and Lurdes Orvalho

*Serviço de Imagiologia, Hospital da Luz, Avenida Lusíada, 100, Lisboa 1500-650, Portugal*

Pedro Vaz

*Centro de Ciências e Tecnologias Nucleares, Instituto Superior Técnico, Universidade de Lisboa, Estrada Nacional 10, km 139,7, Bobadela LRS 2695-066, Portugal*

(Received 2 December 2014; revised 25 March 2015; accepted for publication 25 April 2015; published 9 June 2015)

**Purpose:** Due to its capability to more accurately detect deep lesions inside the breast by removing the effect of overlying anatomy, digital breast tomosynthesis (DBT) has the potential to replace the standard mammography technique in clinical screening exams. However, the European Guidelines for DBT dosimetry are still a work in progress and there are little data available on organ doses other than to the breast. It is, therefore, of great importance to assess the dosimetric performance of DBT with respect to the one obtained with standard digital mammography (DM) systems. The aim of this work is twofold: (i) to study the dosimetric properties of a combined DBT/DM system (MAMMOMAT Inspiration Siemens®) for a tungsten/rhodium (W/Rh) anode/filter combination and (ii) to evaluate organs doses during a DBT examination.

**Methods:** For the first task, measurements were performed in manual and automatic exposure control (AEC) modes, using two homogeneous breast phantoms: a PMMA slab phantom and a 4 cm thick breast-shaped rigid phantom, with 50% of glandular tissue in its composition. Monte Carlo (MC) simulations were performed using Monte Carlo *N*-Particle eXtended v.2.7.0. A MC model was implemented to mimic DM and DBT acquisitions for a wide range of x-ray spectra (24–34 kV). This was used to calculate mean glandular dose (MGD) and to compute series of backscatter factors (BSFs) that could be inserted into the DBT dosimetric formalism proposed by Dance *et al.* Regarding the second aim of the study, the implemented MC model of the clinical equipment, together with a female voxel phantom (“Laura”), was used to calculate organ doses considering a typical DBT acquisition. Results were compared with a standard two-view mammography craniocaudal (CC) acquisition.

**Results:** Considering the AEC mode, the acquisition of a single CC view results in a MGD ranging from  $0.53 \pm 0.07$  mGy to  $2.41 \pm 0.31$  mGy in DM mode and from  $0.77 \pm 0.11$  mGy to  $2.28 \pm 0.32$  mGy in DBT mode. Regarding the BSF, the results achieved may lead to a MGD correction of about 6%, contributing to the improvement of the current guidelines used in these applications. Finally, considering the MC results obtained for the organ dose study, the radiation doses found for the tissues of the body other than the breast were in the range of tens of  $\mu\text{Sv}$ , and are in part comparable to the ones obtained in standard DM. Nevertheless, in a single DBT examination, some organs (such as lung and thyroid) receive higher doses (of about 9% and 21%, respectively) with respect to the CC DM acquisition.

**Conclusions:** Taking into account an average breast with a thickness of 4.5 cm, the MGDs for DM and DBT acquisitions were below the achievable value (2.0 mGy) defined by the European protocol. Additionally, in the case of a fusion imaging study (DM+DBT), the MGD for a 4.5 cm thick breast is of the order of  $1.88 \pm 0.36$  mGy. Finally, organ dose evaluations underline the need to improve awareness concerning dose estimation of DBT exams for some organs, especially when radiation risk is assessed by using the effective dose. © 2015 American Association of Physicists in Medicine. [<http://dx.doi.org/10.1118/1.4921362>]

Key words: breast tomosynthesis, Monte Carlo simulations, breast dosimetry, backscatter factors, radiation organ doses

## 1. INTRODUCTION

Breast cancer is the primary cause of cancer death among women in developing countries, accounting for more than  $1 \times 10^6$  new cancer cases and more than 450 000 deaths annually.<sup>1</sup> Digital mammography (DM) has been demonstrated to be the most effective imaging modality in breast cancer detection, being widely used in screening programs. Nevertheless, the detection of breast lesions using this technique is limited by the obscuring effect of overlapping breast tissue, produced by the projection of a three-dimensional (3D) object (the tumor mass) onto a plane.<sup>2-4</sup> The superposition of normal tissue reduces the capability of detecting cancers and consequently the sensitivity of mammography, particularly in woman with radiographically dense breasts.<sup>5</sup> It can also create image artifacts in a mammogram, which increase false-positive rate and reduce the specificity of DM.

To overcome these limitations, digital breast tomosynthesis (DBT) is an emerging and promising 3D modality for breast imaging, which involves the acquisition of low dose projections by rotating an x-ray tube around the stationary compressed breast in a limited angular range.<sup>6,7</sup> Using specific algorithms, these projections are reconstructed into slices parallel to the image detector, which can be displayed individually.<sup>4,8</sup> The clinical use of DBT in the USA has already been approved by the Food and Drug Administration (FDA) for Hologic<sup>®</sup> Selenia Dimensions and GE Healthcare<sup>®</sup> Seno-Claire systems. The applicability of breast tomosynthesis for screening purposes is still under investigation, but some prospective studies<sup>9,10</sup> show the potential benefits of adding DBT to DM in breast cancer screening.

Screening of the healthy female population implies a comprehensive understanding of some dosimetric aspects related to breast imaging technologies. In this field, the radiation dose in the glandular tissue is one of the major concerns, since it is the tissue at risk of cancer development. To this end, the mean glandular dose (MGD) has been used as the dosimetric quantity for dose estimation in breast dosimetry.<sup>4,6</sup> It has been argued that DBT involves cancer risks that are one to two times higher than digital or screening-film mammography. This assessment was performed through cohort studies of the Biologic Effects of Ionizing Radiation (BEIR) VII Group, where specific sex and age criteria were taken into account for the assessment of cancer risk.<sup>11</sup>

Monte Carlo (MC) modeling and simulations play a fundamental role in dose assessment and optimization of exposure settings both in mammography<sup>12,13</sup> and DBT.<sup>14-17</sup> Regarding breast tomosynthesis dosimetry protocols, the AAPM Task Group 223 report<sup>18</sup> discusses a methodology to estimate the MGD from a tomosynthesis acquisition. For the European Guidelines, the available EUREF dosimetric protocol for DBT (Ref. 19) is still in development and acts as an extension of the UK, European, and IAEA standard protocols for conventional mammography. This methodology introduces the “tomo” factors, *t*-factors (*t*), and *T*-factors (*T*) for the calculation of the breast dose for a single projection and for a complete exposure series, respectively. Note that this formalism only takes into account the incident free in

air kerma ( $K_{\text{air}}$ ) at the surface of the breast, measured in the  $0^\circ$  position, without the backscattered radiation from the breast. Another dosimetric quantity used (both in DM and DBT) is the entrance surface dose (ESD) which refers to the absorbed dose in air, with the contribution of backscattered radiation from the phantom at a point on the surface of the phantom or female breast. When ESD measurements are performed for patients or for a test phantom simulating the breast using, for example, thermoluminescent dosimeters (TLD), the backscatter properties of the phantom material become important.<sup>20</sup>

Currently available data for the dose received from a DBT exam by nonbreast tissue are limited. To our knowledge, only one study has been published on the organ radiation doses from a mammographic procedure, using MC simulations and a female mathematical phantom (Cristy).<sup>21</sup> Determination of the organ doses during a DBT acquisition will allow collection of information for epidemiologic studies of radiation-related diseases and the assessment of the radiological risk involved with DBT. Additionally, these data for organ doses will contribute to the safety assessment of DBT examinations performed during pregnancy.<sup>21</sup>

This study aims to characterize the dosimetric performance of a clinical DBT system, using a W/Rh target/filter combination, and at assessing organ doses during a DBT examination. In order to understand the magnitude of the backscattered radiation in a 3D breast imaging modality, the calculation of the backscattering factors (BSF)<sup>22</sup> in DBT and DM mode was performed. To the best of our knowledge, no BSF values have previously been reported in the literature for a DBT acquisition mode with the option of W/Rh target/filter combination.

To reach the aforementioned objectives, a set of dose measurements were performed with a dual imaging DBT/DM acquisition system in a Portuguese hospital. Additionally, MC calculations were performed, mimicking the DBT acquisition process, for different voltages (in the range between 24 and 34 kVp, in 2 kVp steps), considering the W/Rh target/filter combination and different breast thicknesses (2, 4, 6, and 8 cm). The developed MC tool was used together with the female voxel phantom “Laura” to perform a detailed study of the organ doses in DBT.

## 2. METHODS AND MATERIALS

For the dose measurements, the MAMMOMAT Inspiration system (Siemens<sup>®</sup>)<sup>23</sup> available in Hospital da Luz, Lisbon, Portugal was used. This equipment has a dual imaging functionality, since it performs both DBT and DM image acquisitions, allowing direct dose comparisons between both breast imaging techniques. The target/filter combinations available for DM examinations are Mo/Mo and W/Rh, while for DBT examinations, only the second combination is accessible. For this reason, the dosimetric comparisons between DM and DBT presented in this study were only performed taking into account the W/Rh target/filter combination. Also, in digital systems, this combination offers better performances in terms of image quality at a lower dose. Several studies<sup>13,24</sup>

TABLE I. Summary of the characteristics of the Siemens MAMMOMAT Inspiration system (adapted from Ref. 4).

| Siemens MAMMOMAT inspiration system |                          |
|-------------------------------------|--------------------------|
| Detector type                       | Full field-direct (a-Se) |
| Detector size (cm)                  | 24×30                    |
| Detector motion                     | Static                   |
| X-ray tube target                   | W                        |
| X-ray tube filtration               | 0.05 mm Rh               |
| X-ray tube motion                   | Continuous               |
| Angular range (deg)                 | 50                       |
| Number of projections               | 25                       |
| Source to detector distance (cm)    | 65.5                     |
| Development stage                   | Commercial system        |

have pointed out that, when studying digital systems with Selenium detectors, the W/Rh anode/filter combination maximizes the figure of merits (FOMs) for contrast-to-noise ratio (CNR) generally used in mammographic optimization studies (i.e.,  $CNR^2/MGD$ ). The characteristics of the breast tomosynthesis clinical system used are shown in Table I.

Measurements were undertaken for two different acquisition modalities: manual mode, which allows for the selection of the tube voltage and the current-exposure time product (mAs), and automatic exposure control (AEC) mode, which enables voltage selection ensuring the optimal exposure of the image detector and compensating for the breast thickness and composition.

## 2.A. Air kerma measurements with ionizing chamber

To perform the measurements, a SFD mammographic ionization chamber (IC) (type 34069, PTW-Freiburg<sup>®</sup>) was used. The IC has a sensitive volume of 6 cm<sup>3</sup> and was previously calibrated with an associated uncertainty of 5%. To measure the ESD, the IC was placed above a 4 cm thick breast-shaped rigid phantom (MTM 100/100R, CIRS<sup>®</sup>), with a homogeneous composition of 50% glandular/50% adipose tissue, coated with a 5 mm layer of 100% adipose tissue. The following parameters for the clinical equipment were selected for MC validation purposes: W/Rh anode/filter combination, 100 mAs, and a range of tube voltages between 24 and 34 kVp, in 2 kVp steps. To obtain the results for  $K_{air}$ , the same set of

measurements was repeated without the phantom between the compression plate and the detector, maintaining the IC at the same height.

For the AEC measurements, a mammographic phototimer consistency phantom (model 159A, GAMMEX<sup>®</sup>) was used. This is composed by seven PMMA slabs with different thicknesses: 2, 4, 6, and 7 cm.

## 2.B. Monte Carlo simulations

The state-of-the-art Monte Carlo *N*-Particle eXtended (MCNPX) program version 2.7.0 (Ref. 25) was used for photon and electron transport simulation, and a DM/DBT computational model was implemented to perform dose calculations for the determination of both MGD and BSF. In order to compute the organ doses from a DBT examination, a representation of the human body, based on the female reference voxel phantom Laura, was used in the simulations.

The F6 tally in MCNPX represents the energy deposition over a defined volume (in MCNPX called “cell”) and can be employed in situations in which charged particle equilibrium (CPE) is valid. Since the energy range of the x-ray photons is relatively low in diagnostic and the tally volume considered in the present work is large with respect to the electron range,<sup>25</sup> it can be assumed that the condition of CPE is satisfied in the breast tissue. Hence, the absorbed dose is equal to the collision kerma and the energy locally transferred to the electrons is absorbed at the interaction site. Therefore, only the photon physics mode of the MC code was used<sup>25</sup> and F6 tallies were adopted to perform all the dose calculations mentioned in the present study.

### 2.B.1. Geometrical model

The simplified geometrical model implemented in MCNPX is shown in Fig. 1, mimicking the experimental setup adopted for the IC measurements. Considering the different distributions of glandular tissue in female breasts, an average breast is defined as being 4–5 cm thick, with an outer skin layer of 0.5 cm, and an interior composed of a homogeneous mixture of 50% adipose and 50% glandular tissue, where the MGD is estimated.<sup>4,26,27</sup> The phantom of the compressed breast was modeled as a semicircular cylinder with 8.75 cm radius,<sup>28</sup> at

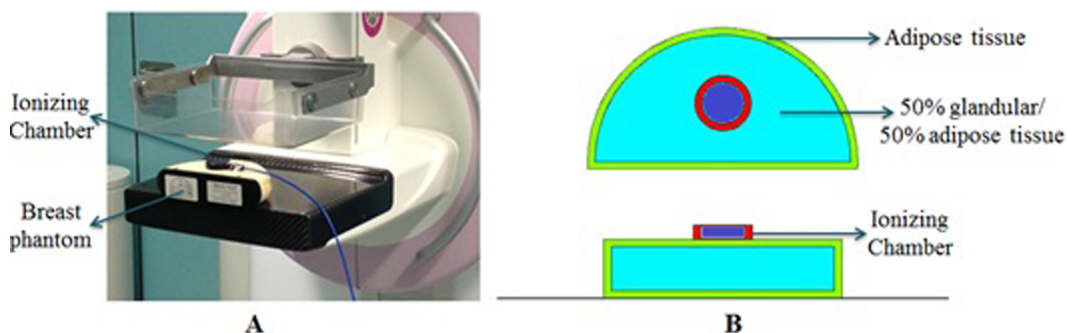


FIG. 1. Representation of the experimental setup used during the IC measurements (A) and the geometry adopted for the MCNPX simulations, in top and profile views (B).

four different thicknesses: 2, 4, 6, and 8 cm. The composition of the phantom was defined as a homogeneous mixture of 50% glandular and 50% adipose tissue, surrounded by a 5 mm layer of adipose tissue.<sup>29</sup> The IC was modeled as a cylinder with 2 cm radius and 1 cm height, with a sensitive volume of 6 cm<sup>3</sup> of air.

The MC model included an x-ray isotropic point source, as an approximation of the focal spot of the x-ray tube, which was collimated into a cone to ensure the emission in the direction of the detector. The source-to-image distance (SID) was set at 65 cm, for the 0° DBT projection. Each simulated DBT examination consisted of a set of 25 projections, over an angular range from -24° to +24°, in 2° steps. A wide range of polychromatic x-ray spectra was considered, between 24 and 34 kVp, in 2 kVp steps for a W target and a filter with 0.05 mm of Rh. The spectral data used as input source were obtained through the simulation tool developed by Boone and Seibert,<sup>30</sup> which generates x-ray spectra typically used for applications in diagnostic radiology and mammography. In these catalogues, the uncertainty in photon fluence, and spatial and energy distribution, is expected to be 10%–15%.<sup>31</sup> For all the simulations,  $5 \times 10^8$  particle histories were run, leading to a statistical uncertainty of about 2% in the results.

### 2.B.2. Voxel phantom for organ dose assessment in DBT

To assess the organ doses during a DBT acquisition [in a craniocaudal (CC) view], MC simulations including the female voxel computational phantom Laura were used. Mathematical phantoms describe internal organs shapes and the outer body contour using surface equations. These have limitations in their ability to describe complex 3D shapes. In contrast, voxel phantoms are based on segmented images from CT or magnetic resonance imaging (MRI), providing a more realistic replication of human anatomy.<sup>32</sup>

Laura was developed by GSF-National Research Center for Environment and Health (Germany) and was constructed from a whole body CT scan of a 43 yr old female patient of 167 cm height and 59 kg weight (ICRP reference values: 163 cm and 60 kg). The voxel size is 5 mm height with an in-plane resolution of 1.875 mm, which corresponds to a voxel volume of 17.6 mm<sup>3</sup>.<sup>33</sup> The organs that were taken into account during a general DBT/DM examination are reported in Table II.

This type of voxel phantom is created when the individuals are in a supine posture, so some difference in organ shape and position can be envisaged.<sup>34</sup> For this reason, in Laura's voxel phantom implementation, some geometric modifications were made. The head of the phantom was removed, since it was inside the primary x-ray field, which does not happen during a real DBT acquisition. In addition, the MC simulation included a breast compression plate, a breast support plate, and the image detector, whose material composition is shown in Table III.<sup>29</sup> The geometry implemented can be seen in Fig. 2.

It is generally assumed that the MGD delivered during DBT is approximately the same of a one-view standard DM acquisition<sup>19</sup> which, according to the European guidelines for

TABLE II. Organs and masses that were considered for the radiation organ dose calculations.

| Organ phantom | Mass (g) |
|---------------|----------|
| Breast        | 502.00   |
| Ovaries       | 11.30    |
| Liver         | 1334.00  |
| Thyroid       | 24.75    |
| Uterus        | 82.50    |
| Left lung     | 305.80   |
| Right lung    | 375.78   |
| Left kidney   | 172.31   |
| Right kidney  | 108.14   |

quality assurance in breast cancer screening, is 2.0 mGy,<sup>35</sup> given an average breast thickness of 4.5 cm. As such, the dose to each organ from a complete DBT examination was calculated considering a fixed MGD value of 2.0 mGy for the female breast.

### 2.C. Dosimetric formalism in DM and DBT

In this work, the dosimetric formulation related to the European Guidelines for quality assurance in breast cancer screening<sup>35</sup> was considered, both for DM and DBT. The MGD for a DM examination (MGD<sub>DM</sub>) is determined using the following expression:

$$\text{MGD}_{\text{DM}} = K \times g \times c \times s, \quad (1)$$

where  $g$  and  $c$  are conversion factors related with the glandularity of the breast and the  $s$ -factor is related to the x-ray spectra. These multiplicative factors are tabulated in the extensive work by Dance *et al.*<sup>14,28,36</sup>  $K$  is the incident air kerma, measured at the upper surface of the phantom or female breast without the backscatter effect.

In DBT, the MGD is the sum of the doses received from individual projections.<sup>19</sup> As an extension of the existing standard protocols, the DBT dosimetric formalism<sup>14</sup>

$$\text{MGD}(\theta)_{\text{DBT}} = K \times g \times c \times s \times t(\theta) \quad (2)$$

gives the MGD( $\theta$ )<sub>DBT</sub> for the projection at angle  $\theta$  and  $t(\theta)$  is the tomofactor at this angle.  $K$  is the incident air kerma, measured at the upper surface of the phantom at 0° projection (x-ray vertical above the breast), without the backscatter effect, and for the current-time product (mAs) applied at projection  $\theta$ . The  $t$ -factor  $t(\theta)$  is calculated using

TABLE III. Material composition and densities of the breast compression plate, breast support plate, and the image detector of the model implemented with MCNPX.

| Structure            | Material | Density (g/cm <sup>3</sup> ) |
|----------------------|----------|------------------------------|
| Compression plate    | PMMA     | 1.2                          |
| Breast support plate | Carbon   | 1.7                          |
| Image detector       | Selenium | 4.5                          |

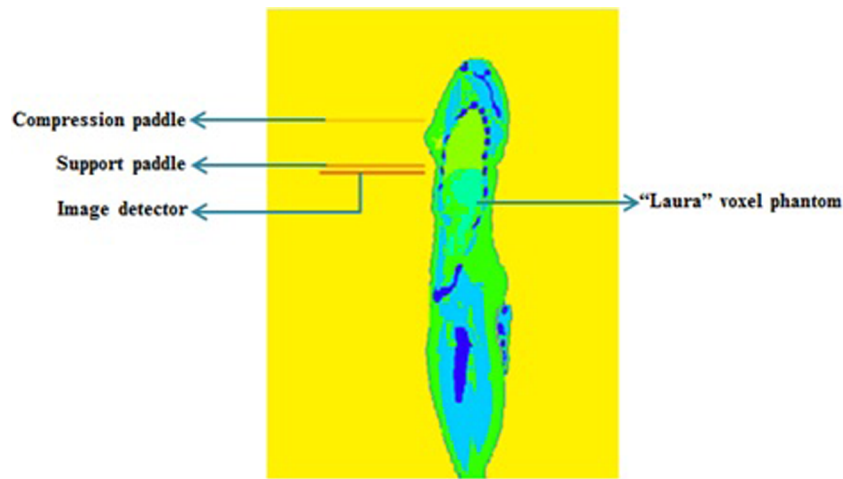


FIG. 2. Voxel phantom setup without head is shown. This configuration was used to calculate the doses for all the organs reported in Table II. The compression paddle, breast support, and image detector were also simulated.

$$t(\theta) = \frac{\text{MGD}(\theta)}{\text{MGD}(0)}, \quad (3)$$

where the  $\text{MGD}(0)$  at  $0^\circ$  is the same as the one for mammography using the same tube loading and energy spectrum, so at this projection,  $t(\theta)$  is 1.<sup>14,19</sup>

In a complete DBT examination,<sup>14,19</sup> the  $\text{MGD}_{\text{DBT}}$  is determined using

$$\text{MGD}_{\text{DBT}} = K_T \times g \times c \times s \times T, \quad (4)$$

where  $K_T$  is the incident air kerma measured at  $0^\circ$  but for the total tube loading for the complete exam.  $T$  is the  $T$ -factor<sup>14,19</sup> for the complete exam and is given by

$$T = \sum_i \alpha_i t(\theta_i). \quad (5)$$

The summation in Eq. (5) is over all the projections for the examination and  $\alpha_i$  refers to the fraction of the total mAs for the different projections. In the case of the same tube loading for each projection,  $T$  is calculated using the expression

$$T = \frac{1}{N} \sum_i t(\theta_i), \quad (6)$$

where  $N$  is the number of projections.

$\text{MGD}$  can be determined from  $K_T$  or from  $\text{ESD}$ , measured with an IC. In this last case, a correction factor  $1/\text{BSF}$  should be applied in order to remove the backscatter effect.  $\text{BSF}$  was calculated for each x-ray spectrum and for both DM and DBT acquisition modes, according to the following expression:

$$\text{BSF} = \frac{\text{ESD}}{K_{\text{air}}}, \quad (7)$$

where  $\text{ESD}$  and  $K_{\text{air}}$  (air kerma free in air) were obtained with  $\text{mcNpX}$  simulations with and without the breast phantom, respectively. In this way, whenever it is not possible to obtain  $K_{\text{air}}$ ,<sup>22</sup> for a DM examination, the  $\text{MGD}_{\text{DM}}$  is given by

$$\text{MGD}_{\text{DM}} = \text{ESD} \times g \times c \times s \times \frac{1}{\text{BSF}}. \quad (8)$$

For a complete DBT acquisition, a total  $\text{BSF}$  ( $\text{BSF}_T$ ) was determined and the  $\text{MGD}_{\text{DBT}}$  is calculated by

$$\text{MGD}_{\text{DBT}} = \text{ESD}_T \times g \times c \times s \times T \times \frac{1}{\text{BSF}_T}, \quad (9)$$

where  $\text{BSF}_T$  is the sum of the  $\text{BSF}$  obtained in each of the 25 projections and  $\text{ESD}_T$  is the  $\text{ESD}$  for a complete examination measured at the upper surface of the phantom.

For the estimation of the  $\text{MGD}$  with MC calculations in DM and DBT, Eqs. (1) and (4), respectively, were used. In the DBT case, the air kerma  $K$  was computed by modeling the IC, without the breast phantom and for each angular projection. As such,  $K_T$  in Eq. (4) results from the sum of the 25 projection views. Moreover, the  $T$ -factors, for each spectrum and breast thickness evaluated, were obtained by  $\text{mcNpX}$  calculations as ratio of absorbed doses within the adipose-glandular mixture breast tissue and used for the  $\text{MGD}_{\text{DBT}}$  calculations. For the remaining multiplicative parameters ( $g$ ,  $c$ , and  $s$  factors) used in Eqs. (1) and (4), the tabulated values of Dance *et al.* were used.<sup>14,28,36</sup>

### 3. RESULTS

#### 3.A. MC model validation

Measurements were performed by placing the IC at the center of the breast phantom and the entire system (breast phantom, IC, and x-ray focusing tube) was aligned to the  $0^\circ$  projection angle. The same alignment was implemented in the MC model used for calculations.

The  $\text{ESD}$  and  $K_{\text{air}}$  measurements, as well as the simulated results for DBT acquisition, are displayed in Table IV, for all the tube voltages considered in this part of the study. For  $\text{ESD}$ , taking into account both measurements and simulations, the smallest difference was achieved for 24 kVp (1.60% difference), while the highest discrepancy was registered for 28 kVp (2.65% difference). Regarding the  $K_{\text{air}}$  results obtained from free in air measurements and from  $\text{mcNpX}$  calculations, the higher difference was verified for 32 kVp (4.65%

TABLE IV. Comparison between the ESD and  $K_{\text{air}}$  measurements performed without the breast phantom and the MCNPX simulation results in DBT mode. The current-exposure time product selected in all cases was 100 mAs. The uncertainty related to measurements is 5% and to the MC simulations is 2%.

| Tube voltage (kVp) | ESD <sub>measured</sub> (mGy) | ESD <sub>simulated</sub> (mGy) | Relative difference (%) | $K_{\text{air-measured}}$ (mGy) | $K_{\text{air-simulated}}$ (mGy) | Relative difference (%) |
|--------------------|-------------------------------|--------------------------------|-------------------------|---------------------------------|----------------------------------|-------------------------|
| 24                 | 2.140 ± 0.107                 | 2.174 ± 0.043                  | -1.574                  | 2.120 ± 0.106                   | 2.041 ± 0.041                    | 3.703                   |
| 26                 | 2.190 ± 0.146                 | 2.983 ± 0.060                  | -2.504                  | 2.890 ± 0.145                   | 2.786 ± 0.056                    | 3.582                   |
| 28                 | 3.630 ± 0.182                 | 3.726 ± 0.075                  | -2.647                  | 3.600 ± 0.180                   | 3.478 ± 0.070                    | 3.394                   |
| 30                 | 4.345 ± 0.217                 | 4.436 ± 0.089                  | -2.103                  | 4.295 ± 0.215                   | 4.122 ± 0.082                    | 4.019                   |
| 32                 | 5.050 ± 0.253                 | 5.135 ± 0.103                  | -1.691                  | 4.990 ± 0.250                   | 4.758 ± 0.095                    | 4.647                   |
| 34                 | 5.765 ± 0.288                 | 5.907 ± 0.118                  | -2.468                  | 5.680 ± 0.284                   | 5.473 ± 0.109                    | 3.645                   |

difference) and the lower for 28 kVp (3.40% difference). The uncertainties associated with the dose measurements are related to the uncertainty of the mammographic IC (5%), while the simulation results present a statistical uncertainty of 2%.

Concerning the DM acquisition mode, the ESD and  $K_{\text{air}}$  results obtained from the IC measurements and from the MC simulations are shown in Table V, for all tube voltages considered. The smallest relative difference between measured and simulated ESD results was obtained for 26 kVp (0.07% difference), whereas the greatest discrepancy was registered for 30 kVp (1.60% difference). Comparing the experimental and the simulated  $K_{\text{air}}$  values, the smallest relative difference was achieved for 24 kVp (0.90% difference), while for 30 kVp, a higher relative difference was observed (3.61%).

A good agreement between the ESD and  $K_{\text{air}}$  experimental values and MC simulation results is achieved, at the level of 5% (uncertainty associated with the IC). As such, it can be considered that the implemented computational model accurately reproduces the clinical DM/DBT system.

### 3.B. MGD assessment in DBT and DM

The MGDs in the two acquisition modes were assessed from both measurements and computational results, taking into account exactly the same exposure parameters and x-ray spectra mentioned in Sec. 2.A. To calculate the MGD, the dosimetric formalisms proposed by Dance *et al.* were followed, both for DM (Refs. 28 and 36) and DBT acquisitions,<sup>14</sup> as described in Sec. 2.C. The conversion factors  $c$  ( $c = 1.000$ ) and  $s$  [ $s(W/Rh) = 1.042$ ] were obtained from the published literature.<sup>28,36</sup> The  $g$ -factors were determined at each peak tube voltage (24–34 kVp), considering also the ones calculated by Dance.<sup>36</sup>

In this work, the tomo factors were calculated with MCNPX simulations for each peak tube voltage (24–34 kVp) and for the different breast thicknesses (2, 4, 6, and 8 cm), considering an angular range between  $-24^\circ$  and  $+24^\circ$ , in  $2^\circ$  increments. Dance *et al.* also calculated these values for the dose estimations in DBT and tabulated  $t$ -factors for each breast thickness and projection angle reported.<sup>14</sup> The  $t$ -factors published by Dance *et al.* were obtained as an average between maximum and minimum values found for different x-ray spectra. For this reason, in order to obtain more precise results, the  $t$ -factors were calculated for different spectra, and the results are presented in Fig. 3. As an example, the results achieved for a breast thickness of 4 cm show a good agreement with the ones calculated by Dance *et al.*,<sup>14</sup> especially when considering projection angles below  $10^\circ$ – $12^\circ$ . For wider angles and higher voltages, the discrepancies with the Dance *et al.* values are slightly larger. Similar trends were obtained also for the remaining thicknesses. The statistical uncertainty associated with the calculated MC  $t$ -factors was of the order of 3% for all the projections.

Additionally, in Table VI, the  $T$ -factors calculated with MCNPX simulations are reported with a statistical uncertainty of about 3%. These parameters were applied to the DBT dosimetric formalism described in Eq. (4), in order to obtain the  $MGD_{\text{DBT}}$  from both measurements and simulations.

As a first step, the MGDs obtained from measurements, for the two imaging modalities, were compared, taking into consideration the different tube voltages (24–34 kVp) and a breast thickness of 4 cm. All the acquisitions were performed with the same current-exposure time product (100 mAs). The absolute uncertainty of the  $MGD_{\text{DM}}$  measurements was estimated to be 13%. This value was based on (i) the inherent uncertainty in the determination of  $K_{\text{air}}$  given by the

TABLE V. Comparison between ESD and  $K_{\text{air}}$  measurements performed without the breast phantom versus MCNPX simulation results in DM mode. The current-exposure time product selected in all cases was 100 mAs. The uncertainty related to measurements is 5% and to the MC simulations is 2%.

| Tube voltage (kVp) | ESD <sub>measured</sub> (mGy) | ESD <sub>simulated</sub> (mGy) | Relative difference (%) | $K_{\text{air-measured}}$ (mGy) | $K_{\text{air-simulated}}$ (mGy) | Relative difference (%) |
|--------------------|-------------------------------|--------------------------------|-------------------------|---------------------------------|----------------------------------|-------------------------|
| 24                 | 2.388 ± 0.119                 | 2.407 ± 0.046                  | -0.818                  | 2.278 ± 0.114                   | 2.258 ± 0.044                    | 0.911                   |
| 26                 | 3.222 ± 0.161                 | 3.219 ± 0.063                  | 0.067                   | 3.065 ± 0.153                   | 3.012 ± 0.061                    | 1.716                   |
| 28                 | 4.000 ± 0.200                 | 3.940 ± 0.080                  | 1.501                   | 3.797 ± 0.189                   | 3.683 ± 0.077                    | 3.006                   |
| 30                 | 4.755 ± 0.238                 | 4.680 ± 0.097                  | 1.577                   | 4.512 ± 0.226                   | 4.349 ± 0.093                    | 3.608                   |
| 32                 | 5.478 ± 0.274                 | 5.438 ± 0.114                  | 0.740                   | 5.205 ± 0.260                   | 5.019 ± 0.109                    | 3.566                   |
| 34                 | 6.267 ± 0.313                 | 6.342 ± 0.134                  | -1.200                  | 5.917 ± 0.296                   | 5.843 ± 0.129                    | 1.246                   |

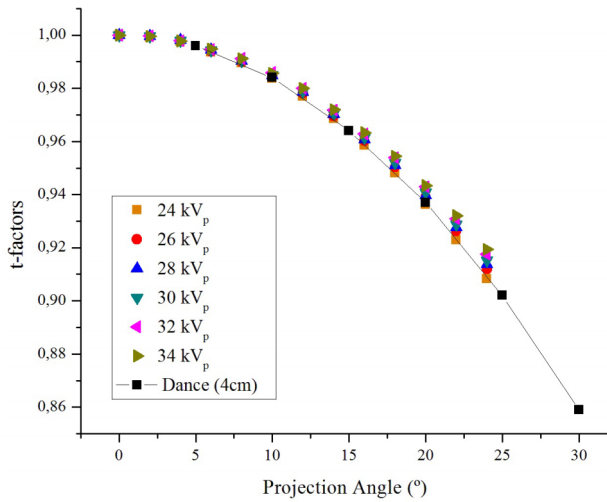


FIG. 3. Comparison between the Dance  $t$ -factors for a 4 cm thick breast and the calculated  $t$ -factors, from  $0^\circ$  to  $+24^\circ$  for each tube voltage (24–34 kVp). The obtained  $t$ -factors have an associated uncertainty of about 3%.

European protocol on dosimetry in mammography ( $\pm 12\%$ ),<sup>37</sup> (ii) uncertainty in the measurement of the  $K_{air}$  using the IC ( $\pm 5\%$ ), and (iii) the error estimations on the conversion factors reported by Dance *et al.*<sup>36</sup> Regarding  $MGD_{DBT}$  measurements, an absolute uncertainty of 14% was achieved, based on the aforementioned uncertainties and the error estimation associated with the  $T$ -factors ( $\pm 2\%$ ). In this way, as shown in Table VII, for DM mode, the MGD varies from  $0.68 \pm 0.09$  mGy to  $2.13 \pm 0.28$  mGy, whereas for DBT mode, the MGD ranges from  $0.61 \pm 0.09$  mGy to  $1.99 \pm 0.28$  mGy.

Table VIII shows the  $MGD_{DM}$ , calculated through MC simulations, considering an energy range between 24 and 34 kVp and the four different breast thicknesses. The absolute uncertainty of  $MGD_{DM}$  was estimated to be 10%, due to the MCNPX statistical uncertainty (which in this case was also  $\pm 2\%$ ), the uncertainty associated to the x-ray spectral data ( $\pm 10\%$ ) and the error estimations on the conversion factors reported by Dance *et al.*<sup>36</sup> Regarding this imaging modality, the  $MGD_{DM}$  varies from  $0.38 \pm 0.04$  mGy to  $3.31 \pm 0.34$  mGy and the results increase with decreasing breast thickness.

Table IX displays the  $MGD_{DBT}$ , obtained with MC calculations, for an energy range between 24 and 34 kVp and the four different breast thicknesses. The absolute uncertainty of  $MGD_{DBT}$  was estimated to be also 10%. In DBT, the

TABLE VII. Comparison between MGD for mammography and for DBT, considering the results obtained with measurements, for a breast thickness of 4 cm and a glandularity of 50%. The uncertainties related to  $MGD_{DM}$  and  $MGD_{DBT}$  are 13% and 14%, respectively.

| Tube voltage (kVp) | $MGD_{DM}$ (mGy) | $MGD_{DBT}$ (mGy) | Difference (%) |
|--------------------|------------------|-------------------|----------------|
| 24                 | $0.68 \pm 0.09$  | $0.61 \pm 0.09$   | 10.04          |
| 26                 | $0.97 \pm 0.13$  | $0.89 \pm 0.12$   | 8.72           |
| 28                 | $1.25 \pm 0.17$  | $1.15 \pm 0.16$   | 8.16           |
| 30                 | $1.54 \pm 0.21$  | $1.42 \pm 0.20$   | 7.75           |
| 32                 | $1.83 \pm 0.24$  | $1.70 \pm 0.24$   | 6.97           |
| 34                 | $2.13 \pm 0.28$  | $1.99 \pm 0.28$   | 6.82           |

maximum  $MGD_{DBT}$  calculated was  $2.97 \pm 0.31$  mGy, while the lower value of  $MGD_{DBT}$  was  $0.32 \pm 0.03$  mGy.

### 3.C. Measurements in AEC

The exposure parameters chosen by the AEC mode for DM and DBT, together with the respective MGDs, are shown in Table X. For all cases evaluated, the AEC selected a higher tube current-exposure time product with increasing PMMA phantom thickness (whereas the glandularity of the equivalent breast decreases).

In case of a single DM CC view acquisition, the  $MGD_{DM}$  calculated given the Dance *et al.* dosimetric formalism<sup>36</sup> can range from  $0.53 \pm 0.07$  mGy to  $2.41 \pm 0.31$  mGy, for the assessed equivalent breast thicknesses. Regarding DBT acquisitions,  $MGD_{DBT}$  can vary from  $0.77 \pm 0.11$  mGy to  $2.28 \pm 0.32$  mGy.

### 3.D. BSF evaluation

In order to study the backscattered radiation in DM and DBT, BSFs were calculated through MCNPX simulations, and measured both in DBT and DM mode for a standard breast of 4 cm thickness, with 50% glandular composition. Table XI shows the measured and calculated BSF values in DM mode, obtained for a range of mammographic x-ray spectra for the four different breast phantom thicknesses. The uncertainties related to  $BSF_{measured}$  refer to the uncertainty of the IC, while the uncertainties of the  $BSF_T$  computed results refer to the statistical uncertainty of the MC calculations. As can be

TABLE VI. MCNPX calculation of the  $T$ -factors for each tube voltage (24–34 kVp) and for the different breast thicknesses assessed (2, 4, 6, and 8 cm), to be applied at the DBT dosimetric formalism. The obtained  $T$ -factors have an associated statistical uncertainty of about 2%.

| Tube voltage (kVp) | Breast thickness (cm) |                   |                   |                   |
|--------------------|-----------------------|-------------------|-------------------|-------------------|
|                    | 2                     | 4                 | 6                 | 8                 |
| 24                 | $0.978 \pm 0.028$     | $0.967 \pm 0.027$ | $0.961 \pm 0.027$ | $0.959 \pm 0.027$ |
| 26                 | $0.979 \pm 0.028$     | $0.968 \pm 0.027$ | $0.962 \pm 0.027$ | $0.961 \pm 0.027$ |
| 28                 | $0.980 \pm 0.028$     | $0.969 \pm 0.027$ | $0.963 \pm 0.027$ | $0.961 \pm 0.027$ |
| 30                 | $0.980 \pm 0.028$     | $0.969 \pm 0.027$ | $0.964 \pm 0.027$ | $0.962 \pm 0.027$ |
| 32                 | $0.981 \pm 0.028$     | $0.970 \pm 0.027$ | $0.965 \pm 0.027$ | $0.963 \pm 0.027$ |
| 34                 | $0.981 \pm 0.028$     | $0.971 \pm 0.027$ | $0.965 \pm 0.027$ | $0.963 \pm 0.027$ |

TABLE VIII. MCNPX calculation of the MGD<sub>DM</sub>, considering a breast thickness of 2, 4, 6, and 8 cm and a breast glandularity of 50%. The uncertainty for MGD<sub>DM</sub> results is of about 10%.

| Tube voltage (kVp) | Breast thickness (cm) |             |             |             |
|--------------------|-----------------------|-------------|-------------|-------------|
|                    | 2                     | 4           | 6           | 8           |
| 24                 | 1.11 ± 0.11           | 0.67 ± 0.07 | 0.50 ± 0.05 | 0.38 ± 0.04 |
| 26                 | 1.54 ± 0.16           | 0.96 ± 0.10 | 0.70 ± 0.07 | 0.54 ± 0.06 |
| 28                 | 1.93 ± 0.20           | 1.22 ± 0.12 | 0.91 ± 0.09 | 0.71 ± 0.07 |
| 30                 | 2.35 ± 0.24           | 1.49 ± 0.15 | 1.10 ± 0.11 | 0.87 ± 0.09 |
| 32                 | 2.79 ± 0.28           | 1.76 ± 0.18 | 1.30 ± 0.13 | 1.04 ± 0.11 |
| 34                 | 3.31 ± 0.34           | 2.11 ± 0.22 | 1.57 ± 0.16 | 1.25 ± 0.13 |

TABLE IX. MCNPX calculation of the MGD<sub>DBT</sub>, considering a breast thickness of 2, 4, 6, and 8 cm and a breast glandularity of 50%. The uncertainty for MGD<sub>DBT</sub> results is of about 10%.

| Tube voltage (kVp) | Breast thickness (cm) |             |             |             |
|--------------------|-----------------------|-------------|-------------|-------------|
|                    | 2                     | 4           | 6           | 8           |
| 24                 | 0.97 ± 0.10           | 0.59 ± 0.06 | 0.42 ± 0.04 | 0.32 ± 0.03 |
| 26                 | 1.39 ± 0.14           | 0.85 ± 0.09 | 0.62 ± 0.06 | 0.48 ± 0.05 |
| 28                 | 1.78 ± 0.18           | 1.11 ± 0.12 | 0.80 ± 0.08 | 0.63 ± 0.07 |
| 30                 | 2.15 ± 0.22           | 1.35 ± 0.14 | 0.98 ± 0.10 | 0.78 ± 0.08 |
| 32                 | 2.54 ± 0.26           | 1.61 ± 0.17 | 1.17 ± 0.12 | 0.93 ± 0.10 |
| 34                 | 2.97 ± 0.31           | 1.91 ± 0.20 | 1.39 ± 0.14 | 1.11 ± 0.12 |

observed, the thickness of the breast seems to have a limited influence on the BSF computed values, but they appear to increase with increasing energy spectrum.

In Table XII, the relative difference between the BSF<sub>measured</sub> and the simulated values for BSF<sub>4cm</sub> is displayed. The results obtained for the IC measurements present a small underestimation with respect to the calculated ones.

Table XIII shows the results of BSF<sub>T</sub>, for a complete breast tomosynthesis examination, taking into account the x-ray spectra generated for the different energies, as well as the different breast thicknesses. The BSF<sub>T-measured</sub> calculated through ESD and K<sub>air</sub> measurements is also presented. The uncertainties associated with BSF<sub>T-measured</sub> are related to the uncertainty of the IC, whereas the uncertainties of the BSF<sub>T</sub> computed results refer to the statistical uncertainty of the MCNPX simulations. As can be seen in this table, the backscatter influence is more pronounced when, for each breast thickness, the tube voltage is increased.

In Table XIV is shown the relative differences between the BSF<sub>T</sub> values, obtained through the measurements performed with the IC, and the BSF<sub>T-4cm</sub> values calculated with the MCNPX simulations.

### 3.E. Organ doses in DBT and DM

The radiation doses received by the organs of the voxel phantom Laura<sup>33</sup> were calculated in the MC calculations considering a W/Rh x-ray spectrum with a voltage of 28 kVp as a source. The x-ray source was aligned with the center of the left breast and the MCNPX simulations were performed for an angular range between -24° and +24°.

In Table XV, the radiation dose received by the organs from a complete DM examination, performed in CC view, is displayed. In this case, the simulations were performed assuming a MGD of 2.0 mGy for the examined breast; subsequently, the radiation doses for other organs were calculated relative to this value. The dose received by the contralateral (CL) breast corresponds to approximately 0.6% of the glandular dose absorbed by the imaged breast. With exception of the CL breast, the organs that absorbed the highest dose levels from DM examinations are the thyroid, left lung (lung near the imaged breast), and liver. Regarding the most distant organs (kidneys, ovaries, and uterus), the dose absorbed is negligible.

In Table XVI, the radiation dose received by the organs is shown, considering a W/Rh 28 kVp x-ray spectrum and half DBT acquisition angular range (from 0° to +24°, in 2° steps). Here, the simulations were performed assuming the same total tube loading (in this case divided for each of the 25 projections) used for the CC DM acquisition previously described. By increasing the projection angle, the glandular dose absorbed by the imaged breast is decreased. The highest dose levels for each projection are received by the thyroid and the left lung, whose dose increases also with increasing projection angle.

## 4. DISCUSSION

### 4.A. MGD assessment in DBT and DM

Regarding the measurements performed for a breast with 4 cm of thickness and 50% of glandular tissue, the MGDs

TABLE X. AEC setting selection (tube voltage and tube current-exposure time product) and MGD calculation for DM and DBT acquisition modes, considering a PMMA phantom thickness of 2, 4, 6, and 7 cm. The equivalent breast thickness and the associated glandularity are also presented (Ref. 19). The uncertainties related to MGD<sub>DM</sub> and MGD<sub>DBT</sub> are 13% and 14%, respectively.

| PMMA phantom thickness (cm) | Equivalent breast thicknesses (cm) | Glandularity of equivalent breast (%) | Exposure (mAs) | DM                 |                         | DBT            |                    |                          |
|-----------------------------|------------------------------------|---------------------------------------|----------------|--------------------|-------------------------|----------------|--------------------|--------------------------|
|                             |                                    |                                       |                | Tube voltage (kVp) | MGD <sub>DM</sub> (mGy) | Exposure (mAs) | Tube voltage (kVp) | MGD <sub>DBT</sub> (mGy) |
| 2                           | 2.1                                | 97                                    | 56             | 24                 | 0.53 ± 0.07             | 71             | 25                 | 0.77 ± 0.11              |
| 4                           | 4.5                                | 41                                    | 80             | 27                 | 0.90 ± 0.12             | 80             | 28                 | 0.98 ± 0.14              |
| 6                           | 7.5                                | 9                                     | 160            | 28                 | 1.65 ± 0.21             | 160            | 30                 | 2.04 ± 0.29              |
| 7                           | 9.0                                | 4                                     | 220            | 29                 | 2.41 ± 0.31             | 180            | 31                 | 2.28 ± 0.32              |

TABLE XI.  $BSF_{\text{measured}}$ , calculated through the IC measurements, and  $BSF$  obtained with MC simulations for DM mode for the following breast thicknesses: 2, 4, 6, and 8 cm.

| Tube voltage (kVp) | $BSF_{\text{measured}}$ | $BSF_{2\text{cm}}$ | $BSF_{4\text{cm}}$ | $BSF_{6\text{cm}}$ | $BSF_{8\text{cm}}$ |
|--------------------|-------------------------|--------------------|--------------------|--------------------|--------------------|
| 24                 | $1.048 \pm 0.052$       | $1.062 \pm 0.021$  | $1.066 \pm 0.021$  | $1.063 \pm 0.021$  | $1.068 \pm 0.021$  |
| 26                 | $1.051 \pm 0.053$       | $1.064 \pm 0.021$  | $1.069 \pm 0.021$  | $1.070 \pm 0.021$  | $1.071 \pm 0.021$  |
| 28                 | $1.054 \pm 0.053$       | $1.065 \pm 0.021$  | $1.070 \pm 0.021$  | $1.066 \pm 0.021$  | $1.068 \pm 0.021$  |
| 30                 | $1.054 \pm 0.053$       | $1.075 \pm 0.021$  | $1.076 \pm 0.021$  | $1.080 \pm 0.022$  | $1.075 \pm 0.022$  |
| 32                 | $1.053 \pm 0.053$       | $1.077 \pm 0.022$  | $1.083 \pm 0.021$  | $1.078 \pm 0.022$  | $1.079 \pm 0.022$  |
| 34                 | $1.059 \pm 0.053$       | $1.081 \pm 0.022$  | $1.085 \pm 0.021$  | $1.085 \pm 0.022$  | $1.084 \pm 0.022$  |

obtained for both DM and DBT, displayed in Table VII, show differences which reach a value of about 10%. This could be in part explained by considering the difference between the two acquisition modalities. In fact, as shown in several studies,<sup>14,18</sup> a variation in DBT dosimetric formalism with respect to the DM one is mainly due to the differences in the geometry adopted for the acquisition process. This issue was addressed by introducing the angle-dependent dose  $t$ -factors that take into account the change in the distance between the tube and the entrance surface of the breast. For example, as shown in the tabulated  $t(\theta)$  values published by Dance *et al.*,<sup>14</sup> for a breast thickness of 4 cm, the MGD calculated at  $25^\circ$  projection decreases by about 10% when compared to the  $0^\circ$  projection, when the same tube loading is considered. Furthermore (as explained in Sec. 4.C), the  $K_{\text{air}}$  measurements introduce some uncertainty inherent to the acquisition process (angular dependence of IC and its calibration factor). Concerning the MCNPX results obtained for the  $MGD_{\text{DM}}$  and  $MGD_{\text{DBT}}$ , displayed in Tables VIII and IX, respectively, when an average breast (4 cm thick with 50% of glandular tissue) is taken into account, the MGDs ranged from  $0.67 \pm 0.07$  mGy to  $2.11 \pm 0.22$  mGy for DM and from  $0.59 \pm 0.06$  mGy to  $1.91 \pm 0.20$  mGy for DBT. In this case, the differences between the two modalities range from 9% to 12%.

The MGD of one view DM acquisition (Tables VIII and IX) is, on average, greater than the one obtained with DBT for each voltage setting with the same exposure parameter (100 mAs). This issue may have some influence on the optimal image quality evaluation for each detection task. For this reason, in order to better evaluate the dosimetric performance of the DBT/DM system, AEC acquisitions for each breast thickness were also analyzed.

TABLE XII. Relative difference between  $BSF_{\text{measured}}$  and  $BSF_{4\text{cm}}$  calculated through MCNPX simulations for DM examination mode.

| Tube voltage (kVp) | Relative difference (%) |
|--------------------|-------------------------|
| 24                 | -1.718                  |
| 26                 | -1.713                  |
| 28                 | -1.518                  |
| 30                 | -2.087                  |
| 32                 | -2.849                  |
| 34                 | -2.455                  |

#### 4.B. AEC measurements

As reported in Table X, the optimal kVp settings for AEC DBT acquisitions are higher than for DM. The higher kVp allows for a lower MGD than would be achievable given the possibility to decrease the mAs when increasing the kVp. Thus, the increased kVp in DBT may be possible due to the tolerance in loss of contrast, allowing for a lower dose and a higher flux, which results in a lower focal spot motion blur due to decreased exposure time. However, in DBT, probably higher energies are needed in order to decrease the quantum noise in each single projection since in this case, the total dose results from the contribution of 25 angular projections. Therefore, in each single projection, the photon fluence reaching the detector is relatively low, causing an increased quantum noise. For this reason, an increase of the tube voltage may be necessary in order to reduce the quantum noise in each single projection (a high quantum noise may lead to a noisy image reconstruction) and to reach the optimal imaging quality for each task considered.

Observing Table X, for an average breast (4.5 cm of equivalent thickness with 41% of glandular tissue), the MGDs for DM and DBT acquisitions were  $0.90 \pm 0.12$  mGy and  $0.98 \pm 0.14$  mGy, respectively, resulting in a difference of about 8.9% between the two modalities. For a thicker breast (9 cm of equivalent thickness), DBT acquisition resulted in a lower MGD (less 5.4% of radiation dose), when compared with the MGD calculated for a DM examination.

Feng and Sechopoulos developed an analogous dosimetric characterization for other clinical DBT equipment, the Hologic Selenia Dimensions.<sup>15</sup> For a single CC view DM acquisition, they reported MGD values ranging from 0.31 mGy, for a 2 cm thick breast, to 5.26 mGy, for an 8 cm thick breast, given various glandular fractions. Concerning DBT, they calculated MGDs ranging from 0.76 mGy, for a 2 cm thick breast, to 3.52 mGy, for an 8 cm thick breast, also for several glandular fractions. Comparing the Feng and Sechopoulos results with the values obtained in this work, an agreement can be observed. The existing variations may be due to the differences that exist between the two clinical systems, due to their operation mode (different angular range, number of projection images, detector movement, and AEC systems). However, the results from both studies present limitations regarding the use of homogeneous breast phantoms and a lack of MGD data from mediolateral oblique (MLO) image acquisitions.<sup>15</sup> Nevertheless, the presented study contributes a

TABLE XIII.  $BSF_{T\text{-measured}}$ , calculated through the IC measurements, and  $BSF_T$  obtained with MC simulations for a complete DBT examination for the following breast thicknesses: 2, 4, 6, and 8 cm.

| Tube voltage (kVp) | $BSF_{T\text{-measured}}$ | $BSF_{T\text{-2cm}}$ | $BSF_{T\text{-4cm}}$ | $BSF_{T\text{-6cm}}$ | $BSF_{T\text{-8cm}}$ |
|--------------------|---------------------------|----------------------|----------------------|----------------------|----------------------|
| 24                 | $1.009 \pm 0.050$         | $1.065 \pm 0.021$    | $1.065 \pm 0.021$    | $1.064 \pm 0.021$    | $1.066 \pm 0.021$    |
| 26                 | $1.007 \pm 0.050$         | $1.071 \pm 0.021$    | $1.070 \pm 0.021$    | $1.069 \pm 0.021$    | $1.071 \pm 0.021$    |
| 28                 | $1.008 \pm 0.050$         | $1.078 \pm 0.022$    | $1.071 \pm 0.021$    | $1.076 \pm 0.022$    | $1.076 \pm 0.022$    |
| 30                 | $1.012 \pm 0.051$         | $1.078 \pm 0.022$    | $1.076 \pm 0.022$    | $1.084 \pm 0.022$    | $1.076 \pm 0.022$    |
| 32                 | $1.012 \pm 0.051$         | $1.078 \pm 0.022$    | $1.079 \pm 0.022$    | $1.081 \pm 0.022$    | $1.084 \pm 0.022$    |
| 34                 | $1.015 \pm 0.051$         | $1.083 \pm 0.022$    | $1.079 \pm 0.022$    | $1.083 \pm 0.022$    | $1.083 \pm 0.022$    |

comparison of the dosimetric characteristics between existing medical equipment used for DBT examinations.

Moreover, as can be seen in Table X, the MGDs achieved for the one-view DM AEC acquisitions are below the achievable values defined by the European protocol<sup>35</sup> for the equivalent breast thicknesses assessed in this part of the study. In case of the 2.1 cm thick breast, the  $MGD_{DM}$  result ( $0.53 \pm 0.07$  mGy) is below the achievable value of 0.6 mGy defined by the European guidelines for a PMMA 2.0 cm thick phantom.<sup>35</sup> The same is observed for the 4.5 and 7.5 cm thick breasts, whose  $MGD_{DM}$  ( $0.90 \pm 0.12$  mGy and  $1.65 \pm 0.21$  mGy, respectively) is below the achievable value of 2.0 mGy for a PMMA 4.5 cm thick phantom.<sup>35</sup> Finally, for the 9 cm thick breast, the  $MGD_{DM}$  value ( $2.41 \pm 0.31$  mGy) is below the achievable value of 5.1 mGy defined for a PMMA 7 cm thick phantom.<sup>35</sup> Regarding DBT, since there are no limiting MGD values yet, the same international established thresholds were considered. In this way, looking at Table X, it can be observed that for all the breast thicknesses evaluated, the MGDs achieved are below the limits mentioned previously.

Fusion imaging studies (DBT plus DM) are a novel aspect of breast examinations that require careful dosimetric assessment. It has been shown that DBT, in combination with DM, increases detection sensitivity while decreasing false-positive and recall rates.<sup>38,39</sup> Taking into account the example of a 4.5 cm thick breast in Table X, the present work shows that a fusion imaging acquisition leads to a MGD of about  $1.88 \pm 0.36$  mGy, which continues to remain below the limit of 2.0 mGy. Dose savings may be achieved if in the future a one-view DBT examination replaces the standard two-view DM screening technique.<sup>15,40,41</sup>

#### 4.C. BSF evaluation

The BSF results obtained for DM mode (Table XI) using a W/Rh clinical system are in good agreement with others

TABLE XIV. Relative difference between  $BSF_{T\text{-measured}}$  and  $BSF_{T\text{-4cm}}$  calculated through MCNPX simulations for DBT examination.

| Tube voltage (kVp) | Relative difference (%) |
|--------------------|-------------------------|
| 24                 | -5.480                  |
| 26                 | -6.312                  |
| 28                 | -6.253                  |
| 30                 | -6.379                  |
| 32                 | -6.646                  |
| 34                 | -6.343                  |

published in the literature for mammography, considering other target/filter combinations. The European Protocol on Dosimetry in Mammography<sup>42</sup> refers BSF values between 1.07 and 1.13, for HVL of 0.25–0.65 mm Al and  $BSF = 1.09$ , in case of lack of HVL information. Similarly to the present work, considering an irradiation setup where no compression plate is simulated, Kramer *et al.* published several values of BSF, taking into account different target/filter combinations:<sup>22</sup> for Mo/Mo, BSF in the range of 1.08–1.10 (HVL of 0.282–0.388 mm Al); for Mo/Rh, BSF in the range 1.09–1.12 (HVL of 0.328–0.433 mm Al); and for Rh/Rh, in the range 1.09–1.14 (HVL of 0.297–0.497 mm Al).

The discrepancy found in Table XII between  $BSF_{\text{measured}}$  and  $BSF_{4\text{cm}}$  calculated through MC simulations for DM examination mode may be explained due to (i) the IC was calibrated only for a voltage of 28 kVp and (ii) only the air kerma free-in-air calibration coefficient was obtained. Rigorous BSF measurements, however, would additionally require the use of the backscatter spectrum so that an air kerma measured at the phantom entrance is included. As also stated in the work of Benmakhlof *et al.*,<sup>43</sup> an accurate BSF could be determined only by MC simulations, since experimentally, BSF evaluation would be excessively time consuming.

For the results achieved in Table XIII for the  $BSF_T$  in a complete DBT examination, when comparing the values of  $BSF_{T\text{-measured}}$  with the computed results for  $BSF_T$ , a small underestimation of the backscatter effect is observed, for all the energies evaluated. Moreover, when comparing the calculated BSF values in Tables XI and XIII, it is possible to note that very small differences in the two acquisition modes are present. This means that in absence of calculated BSFs

TABLE XV. Dose to organs resulting from a complete DM examination, in CC view, for a W/Rh 28 kVp x-ray spectrum calculated through MCNPX simulations.

| Organs          | Dose ( $\mu$ Gy) | MCNPX statistical uncertainty (%) |
|-----------------|------------------|-----------------------------------|
| Examined breast | 2000.000         | 0.080                             |
| CL breast       | 12.000           | 0.080                             |
| Liver           | 15.200           | 0.570                             |
| Ovaries         | —                | —                                 |
| Thyroid         | 273.000          | 0.930                             |
| Uterus          | 0.017            | 70.900                            |
| Left lung       | 385.000          | 0.2                               |
| Right lung      | 21.600           | 0.890                             |
| Left kidney     | 0.404            | 9.850                             |
| Right kidney    | 0.039            | 40.000                            |

TABLE XVI. Dose to organs (in  $\mu\text{Gy}$ ) obtained for half DBT acquisition angular range (from  $0^\circ$  to  $+24^\circ$ , in  $2^\circ$  steps) and for a W/Rh 28 kVp x-ray spectrum, calculated through MCNPX simulations.

| Organs          | $0^\circ$  | $2^\circ$  | $4^\circ$  | $6^\circ$  | $8^\circ$  | $10^\circ$ | $12^\circ$ |
|-----------------|------------|------------|------------|------------|------------|------------|------------|
| Examined breast | 80.100     | 77.800     | 75.949     | 74.188     | 72.774     | 71.364     | 70.205     |
| CL breast       | 0.480      | 0.466      | 0.456      | 0.444      | 0.432      | 0.426      | 0.420      |
| Liver           | 0.606      | 0.600      | 0.576      | 0.533      | 0.492      | 0.454      | 0.417      |
| Ovaries         | —          | —          | —          | —          | —          | —          | —          |
| Thyroid         | 10.900     | 11.700     | 12.070     | 12.159     | 12.794     | 13.097     | 13.513     |
| Uterus          | 0.001      | 0.001      | 0.001      | —          | —          | —          | —          |
| Left lung       | 15.400     | 15.600     | 15.888     | 16.066     | 16.269     | 16.546     | 16.839     |
| Right lung      | 0.863      | 0.864      | 0.844      | 0.823      | 0.830      | 0.845      | 0.835      |
| Left kidney     | 0.016      | 0.014      | 0.014      | 0.015      | 0.015      | 0.015      | 0.013      |
| Right kidney    | 0.002      | 0.001      | 0.002      | 0.001      | 0.001      | 0.000      | 0.001      |
| Organs          | $14^\circ$ | $16^\circ$ | $18^\circ$ | $20^\circ$ | $22^\circ$ | $24^\circ$ |            |
| Examined breast | 69.100     | 68.031     | 67.242     | 66.475     | 65.781     | 65.118     |            |
| CL breast       | 0.414      | 0.408      | 0.402      | 0.396      | 0.396      | 0.390      |            |
| Liver           | 0.396      | 0.371      | 0.359      | 0.340      | 0.325      | 0.311      |            |
| Ovaries         | —          | —          | —          | —          | —          | —          |            |
| Thyroid         | 13.900     | 14.455     | 15.071     | 15.818     | 16.428     | 17.096     |            |
| Uterus          | —          | —          | —          | —          | —          | —          |            |
| Left lung       | 17.100     | 17.307     | 17.556     | 17.709     | 17.921     | 18.146     |            |
| Right lung      | 0.842      | 0.858      | 0.872      | 0.862      | 0.879      | 0.888      |            |
| Left kidney     | 0.017      | 0.014      | 0.017      | 0.013      | 0.013      | 0.011      |            |
| Right kidney    | 0.001      | —          | —          | —          | —          | —          |            |

in DBT mode and for the W/Rh anode/filter combination, the DM ones could be used instead. The relative differences of about 6% (see Table XIV) between  $\text{BSF}_{T\text{-measured}}$  and  $\text{BSF}_{T\text{-4cm}}$  calculated with MCNPX simulations can be explained due to two main reasons: (i) weak angular response of the IC used during the dose measurements<sup>44</sup> and (ii) the calibration process of the IC explained previously. This may have influence in the obtained results, since the calibration was performed in the absence of the breast phantom below the IC. However, for a complete DBT exam, the  $\text{BSF}_T$  values achieved are in the same order of those found in standard mammography.<sup>22,42</sup>

#### 4.D. Organ dose in DBT and DM

For DM, the radiation dose to the organs outside the primary x-ray field is minimal (Table XV). The radiation dose received by the uterus is less than  $0.02 \mu\text{Gy}$ , which may represent the dose to the fetus during the first trimester, since the volume of the simulated uterus in this study is still comparable to that of a woman at this stage of the pregnancy.<sup>21</sup> Sechopoulos *et al.* performed an organ dose study in mammography, using a mathematical phantom, where an absorbed dose of  $0.03 \mu\text{Gy}$  for the uterus is reported. Analyzing these data in the same manner as the paper by Sechopoulos *et al.*, it can be concluded that if a patient is submitted to a DBT exam unaware that they were in the first trimester of pregnancy, according to these results, the dose to the fetus is minimal. Nevertheless, any choice regarding the feasibility of such a diagnostic procedure during pregnancy should be carefully determined by expert medical staff.

In Table XVI, a reduction of the glandular dose absorbed by the imaged breast when the projection angle increases was

observed because for steep angulations, part of the examined breast is not totally irradiated by the primary x-ray field. Conversely, the increasing doses received by thyroid and the left lung may be due to the fact that for steep projections, the distance between the radiation source and these organs is reduced. Summing the organ doses in all the 25 projections and assuming the symmetric geometry of the x-ray source relatively to the breast ( $-24^\circ$  to  $+24^\circ$ ), in DBT, some organs receive a greater dose with respect to the DM. For example, in a CC DM, the left lung receives about  $385 \mu\text{Gy}$  (see Table XV), whereas in DBT, the total dose in all projections is about  $421 \mu\text{Gy}$  (see Table XVI). In this case, an increase of about 9% is envisaged for the left lung in DBT. Another evident dose increase in DBT with respect to DM occurs to the thyroid. In DM, the thyroid receives about  $273 \mu\text{Gy}$ , while in DBT, a dose of about  $347 \mu\text{Gy}$  is delivered, registering a dose increase of about 21%. The different geometry acquisition setup between DM and DBT could partially explain these radiation dose differences (as discussed in Sec. 4.A).

Looking at Tables XV and XVI, some organ dose values present high statistical uncertainties, while others are missing. These issues are a consequence of the poor statistics obtained when organs further from the x-ray source were scored in MC simulations (to obtain statistically significant dose value in distant organs is very time consuming). Nevertheless, even in the presence of values with high uncertainty, the assessed doses are quite conservative, given their order of magnitude (of the order of  $\mu\text{Gy}$ ).

The main limitation of this organ dose study refers to the applicability of the voxel phantoms as a representative of the female human body. A voxel phantom is based on CT images of one patient, therefore lacking the anatomical

variability associated with organ size, shape, and location. The boundary of an organ is defined by uneven steps, whereby the anatomical fidelity depends on the voxel size.<sup>45</sup> The computational reference phantom used in the present study aims to match the 50th-percentile population-average values in terms of body height and weight, which is not representative for a large group of people. Since voxel phantoms are associated with a given patient anatomy, they are inflexible regarding anatomic individual variability to represent either a reference 50th-percentile individual, or non-50th-percentile individuals, whose body morphometry differs substantially.<sup>46</sup> These anatomical variations associated with body size and organ shape can cause as much as 100% difference in the estimated organ doses.<sup>45</sup>

Another source of uncertainty that could affect the present results is related to cardiac and respiratory motion of the patient. In the Laura phantom, these effects are not considered. In standard DM, the exam duration is less than a second, since very high photon fluences are used in order to avoid movements of the patients and image blurring. In this case, given the scan time, it is reasonable to affirm that the use of a static geometry, as the one used in the LAURA phantom calculations, represents a good approximation for a standard DM. The situation is different in DBT, where, for example, the scan time of the MAMMOMAT Inspiration system (Siemens®) used for these measurements is around 25 s.<sup>4</sup> Here, the cardiac and respiratory motion, as well as the movement of the patient, could affect the organ dose estimations to a major extent relative to those obtained for DM. Nevertheless, it is difficult to quantitatively estimate the bias introduced by these effects. From the perspective of the present study, the inclusion of cardiac, respiratory, and general movement features in DBT could generate a greater impact in the imaging performances of the acquisition system, especially taking into account that an image-reconstruction process is involved. The use of phantoms able to consider movement, cardiac, and respiratory effects could be an asset. Nevertheless, the use of such sophisticated voxel phantoms remains limited, in part due to the complexity of the computational effort necessary for their development and execution.<sup>45</sup>

## 5. CONCLUSION

The aim of this study was to improve the knowledge about dosimetric issues concerning the DBT technique. For this reason, several dose-related aspects were taken into account and discussed considering a MAMMOMAT Inspiration system (Siemens®) in a Portuguese Hospital.

We have implemented and validated a MC computational model to simulate the DBT acquisition process. The MC model permitted us to study important dosimetric issues such as backscatter factors, angle-dependent doses, and organ doses other than to the breast using the Laura voxel phantom. The model was validated by IC measurements and a good agreement (at a level of 5%) was observed between the MC simulation results and the experimental values.

Considering, the experimental acquisitions performed in AEC mode, for an average breast (4.5 cm thick with 41% of glandular tissue), the MGDs for DM and DBT acquisitions were  $0.90 \pm 0.12$  mGy and  $0.98 \pm 0.14$  mGy, respectively—both below the achievable value (2.0 mGy) defined by the European protocol. Additionally, if it is necessary to perform a fusion imaging study, the MGD is expected to be approximately  $1.88 \pm 0.36$  mGy.

The determination of the BSFs could be useful if *in vivo* MGD estimations are performed during a DBT examination. In such a case, an accurate free-in-air kerma measurement is quite difficult to accomplish, given also the experimental difficulties previously described (i.e., dedicated detectors with angular dependence response). Moreover, in terms of accuracy for a given diagnostic exam, the improvement of the current guidelines used in breast tomosynthesis applications is of paramount importance. This is particularly true for a relatively new technique, as the DBT one, that is being introduced in clinical trials and/or that could replace the DM in screening programs. The MC results obtained in this work confirm that in DBT, as in DM, an average contribution of the back scattered radiation is of the order of 6%. However, in DBT mode, the acquisition at different projections seems not to have too much influence on the final BSF estimation.

The radiation doses to the organs and tissues located outside the primary x-ray field were found to be low. Nevertheless, CL breast, thyroid, left lung (lung near the imaged breast), and liver are the organs that absorbed the highest radiation dose from a complete DBT exam. Additionally, some organs as left lung (the one aligned with the irradiated breast) and the thyroid receive a greater dose in DBT than in DM (about 9% and 21% increase for left lung and thyroid, respectively), when the total tube loading considered in the two techniques is the same. These results underline the need to have a better awareness concerning dose estimation of some organs when DBT exams are performed, especially when radiation risk is assessed by using the effective dose.

It is worth remarking that a similar study was performed with a mathematical phantom<sup>21</sup> for standard mammography. Nevertheless, since we used a voxel phantom, this study strengthens the accuracy of the organ dose calculations by removing, or at least reducing many uncertainties due to the organ shapes. This issue, as above mentioned, is another fundamental point in the perspective to use DBT in screening programs.

In the future, we plan to use the methodology adopted in this work in order to implement a more accurate model of the female breast, where different glandularities will be assessed and MGD calculations for DM and DBT acquired in MLO view will be performed.

## ACKNOWLEDGMENTS

The authors would like to thank the staff in the Imagiology Department of Hospital da Luz, for their support in performing the dose measurements with the IC in a clinical environment, and the team of the Metrology Laboratory of Ionizing Radiation of the IST for IC calibration process. Also, the authors would like to thank Chris Polin and Nathan Wardlow,

from Centre for Plasma Physics of Queen's University, and Christoph Burbidge, from Instituto Superior Técnico, for the useful suggestions in the final version of the paper.

- <sup>a)</sup> Author to whom correspondence should be addressed. Electronic mail: marianabaptista@ctn.ist.utl.pt
- <sup>1</sup> A. Jemal, F. Bray, and F. Jacques, "Global cancer statistics," *Ca-Cancer J. Clin.* **61**, 69–90 (2011).
- <sup>2</sup> L. T. Niklason, "Digital tomosynthesis in breast imaging," *Radiology* **205**, 399–406 (1997).
- <sup>3</sup> J. T. Dobbins and D. J. Godfrey, "Digital x-ray tomosynthesis: Current state of the art and clinical potential," *Phys. Med. Biol.* **48**, 65–106 (2003).
- <sup>4</sup> I. Sechopoulos, "A review of breast tomosynthesis. Part I. The image acquisition process," *Med. Phys.* **40**, 014301 (11pp.) (2013).
- <sup>5</sup> I. Andersson and D. Ikeda, "Breast tomosynthesis and digital mammography: A comparison of breast cancer visibility and BIRADS classification in a population of cancers with subtle mammographic findings," *Eur. Radiol.* **18**, 2817–2825 (2008).
- <sup>6</sup> A. K. W. Ma and D. G. Darambara, "Mean glandular dose estimation using mcNXP for a digital breast tomosynthesis system with tungsten/aluminum and tungsten/aluminum + silver x-ray anode-filter combinations," *Med. Phys.* **35**(12), 5278–5289 (2008).
- <sup>7</sup> M. A. Helvie, "Digital mammography imaging: Breast tomosynthesis and advanced applications," *Radiol. Clin. North Am.* **48**(5), 917–929 (2010).
- <sup>8</sup> M. Males, D. Mileta, and M. Grgic, "Digital breast tomosynthesis: A technological review," in *53rd International Symposium ELMAR, 14–16 September* (2011).
- <sup>9</sup> N. Houssami and P. Skaane, "Overview of the evidence on digital breast tomosynthesis in breast cancer detection," *Breast* **22**, 101–108 (2013).
- <sup>10</sup> S. E. A. Ciatto, "Integration of 3D digital mammography with tomosynthesis for population breast-cancer screening (STORM): A prospective comparison study," *Lancet Oncol.* **14**, 583–589 (2013).
- <sup>11</sup> R. E. Hendrick, "Radiation doses and cancer risks from breast imaging studies," *Radiology* **257**, 246–253 (2010).
- <sup>12</sup> J. M. Boone, "Glandular breast dose for monoenergetic and high-energy x-ray beams: Monte Carlo assessment," *Radiology* **213**, 23–37 (1999).
- <sup>13</sup> P. Bernhardt, T. Mertelmeier, and M. Hoheisel, "X-ray spectrum optimization of full-field digital mammography: Simulation and phantom study," *Med. Phys.* **33**(11), 4337–4349 (2006).
- <sup>14</sup> D. R. Dance, K. C. Young, and R. E. Engen, "Estimation of mean glandular dose for breast tomosynthesis: Factors for use with UK, European and IAEA breast dosimetry protocols," *Phys. Med. Biol.* **56**, 453–471 (2011).
- <sup>15</sup> S. Feng and I. Sechopoulos, "Clinical digital breast tomosynthesis system: Dosimetric characterization," *Radiology* **263**, 35–42 (2012).
- <sup>16</sup> M. Baptista, S. Di Maria, N. Oliveira, N. Matela, L. Janeiro, P. Almeida, and P. Vaz, "Image quality and dose assessment in digital breast tomosynthesis: A Monte Carlo study," *Radiat. Phys. Chem.* **104**, 158–162 (2014).
- <sup>17</sup> S. Di Maria, M. Baptista, M. Felix, N. Oliveira, N. Matela, L. Janeiro, P. Vaz, L. Orvalho, and A. Silva, "Optimal photon energy comparison between digital breast tomosynthesis and mammography: A case study," *Phys. Med.* **30**, 482–488 (2014).
- <sup>18</sup> I. Sechopoulos, J. M. Sabol, J. Berglund, W. E. Bolch, L. Brateman, E. Christodoulou, M. Flynn, W. Geiser, M. Goodsitt, A. Jones, J. Lo, A. Maidment, K. Nishino, A. Nosratieh, B. Ren, W. Segars, and M. Tiedemann, "Radiation dosimetry in digital breast tomosynthesis: Report of AAPM tomosynthesis subcommittee task group 223," *Med. Phys.* **41**, 091501 (10pp.) (2014).
- <sup>19</sup> R. van Engen, H. Bosmans, R. Bouwman, D. Dance, P. Heid, B. Lazzari, N. Marshall, S. Schopphoven, C. Strudley, M. Thijssen, and K. Young, *Protocol for the Quality Control of the Physical and Technical Aspects of Digital Breast Tomosynthesis Systems* (EUREF, The Netherlands, 2013).
- <sup>20</sup> IAEA, "Dosimetry in diagnostic radiology: An international code of practice," Technical Report Series No. 457, 2007.
- <sup>21</sup> I. Sechopoulos, S. Suryanarayanan, S. Vedantham, C. D'Orsi, and A. Karellas, "Radiation dose to organs and tissues from mammography: Monte Carlo and phantom study," *Radiology* **246**, 434–443 (2008).
- <sup>22</sup> R. Kramer, G. Drexler, N. Petoussi-Hens, M. Zankl, and D. Regulla, "Backscatter factors for mammography calculated with Monte Carlo methods," *Phys. Med. Biol.* **46**, 771–781 (2001).
- <sup>23</sup> Siemens, *MAMMOMAT Inspiration—Digital Mammography Platform for Screening, Diagnostics, Biopsy and Tomosynthesis* (Medical Solutions, Erlangen, Germany, 2009).
- <sup>24</sup> P. Baldelli, N. Phelan, and G. Egan, "Investigation of the effect of anode/filter materials on the dose and image quality of a digital mammography system based on an amorphous selenium flat panel detector," *Br. J. Radiol.* **83**, 290–295 (2010).
- <sup>25</sup> D. B. Pelowitz, *mcNXP User's Manual version 2.7.0*, Los Alamos National Security, 2011.
- <sup>26</sup> I. Sechopoulos, K. Biznakova, X. Qin, B. Fei, and S. Feng, "Characterization of the homogeneous tissue mixture approximation in breast imaging dosimetry," *Med. Phys.* **39**, 5050–5058 (2012).
- <sup>27</sup> D. Dance, C. Skinner, and G. Carlsson, "Breast dosimetry," *Appl. Radiat. Isot.* **50**, 185–203 (1999).
- <sup>28</sup> D. Dance, "Monte Carlo calculation of conversion factor for the estimation of mean glandular breast dose," *Phys. Med. Biol.* **35**, 1211–1219 (1990).
- <sup>29</sup> NIST, available: <http://physics.nist.gov/PhysRefData/XrayMassCoef/ElemTab/z34.html>, accessed 14 May 2014.
- <sup>30</sup> J. M. Boone and J. A. Seibert, "An accurate method for computer-generating tungsten anode x-ray spectra from 30 to 140 kV," *Med. Phys.* **24**, 1661–1670 (1997).
- <sup>31</sup> M. Ay, S. Sarkar, M. Shahriari, D. Sardari, and H. Zaidi, "Assessment of different computational models for generation of x-ray spectra in diagnostic radiology and mammography," *Med. Phys.* **32**, 1660–1675 (2005).
- <sup>32</sup> C. Lee, D. Lodwick, J. Hurtado, D. Pafundi, J. Williams, and W. E. Bolch, "The UF family of reference hybrid phantoms for computational radiation dosimetry," *Phys. Med. Biol.* **55**, 339–363 (2010).
- <sup>33</sup> M. Zankl, J. Becker, U. Fill, and N. Petoussi-Hens, "GSF male and female adult voxel models representing ICRP reference man—the present status." The Monte Carlo Method: Versatility Unbounded in a Dynamic Computing World. Chattaanooga, 2005.
- <sup>34</sup> ICRP, "Adult reference computational phantoms. ICRP publication 110," *Ann. ICRP* **39**(2), 1–166 (2009), see <http://www.icrp.org/publication.asp?id=ICRP%20Publication%20110>.
- <sup>35</sup> N. Perry, M. Broeders, C. de Wolf, S. H. R. Törnberg, and L. von Karsa, *European Guidelines for Quality Assurance in Breast Cancer Screening and Diagnosis* (Health & Consumer Protection, European Commission, Luxembourg, 2006).
- <sup>36</sup> D. R. Dance, C. L. Skinner, C. Young, J. R. Beckett, and C. J. Kotre, "Additional factors for the estimation of mean glandular breast dose using the UK mammography dosimetry protocol," *Phys. Med. Biol.* **45**, 3225–3240 (2000).
- <sup>37</sup> I. H. R. Hauge and H. M. Olerud, "Uncertainties involved in the estimation of mean glandular dose for women in the Norwegian Breast Cancer Screening Program (NBCSP)," *Radiat. Prot. Dosim.* **155**, 81–87 (2013).
- <sup>38</sup> G. Gennaro, R. E. Hendrick, and P. Ruppel, "Performance comparison of single-view digital breast tomosynthesis plus single-view digital mammography with two-view digital mammography," *Eur. Radiol.* **23**, 664–672 (2013).
- <sup>39</sup> S. L. Rose, A. L. Tidwell, M. Ice, A. S. Nordmann, R. J. Sexton, and R. Song, "A reader study comparing prospective tomosynthesis interpretations with retrospective readings of the corresponding FFDM examinations," *Acad. Radiol.* **21**, 1204–1210 (2014).
- <sup>40</sup> S. P. Poplak, T. D. Toesteson, C. A. Kogel, and H. M. Nagy, "Digital breast tomosynthesis: Initial experience in 98 women with abnormal digital screening mammography," *Am. J. Roentgenol.* **189**, 616–623 (2007).
- <sup>41</sup> M. J. Michell, R. K. Wasan, A. P. C. Iqbal, D. R. Evans, and J. C. Morel, "Two-view 2D digital mammography versus one-view digital breast tomosynthesis," Royal College of Radiologists Breast Group Annual Scientific Meeting, Brighton, 2010.
- <sup>42</sup> J. Zoetelief, M. Fitzgerald, W. Leitz, and M. Säbel, in *European Protocol on Dosimetry in Mammography* (EUREF, European Commission, Luxembourg, 1996), Vol. 16263 EN.
- <sup>43</sup> H. Benmakhlouf, H. Bouchard, A. Fransson, and P. Andreo, "Backscatter factors and mass energy-absorption coefficient ratios for diagnostic radiology dosimetry," *Phys. Med. Biol.* **56**, 7179–7204 (2011).
- <sup>44</sup> L. R. Bradley, A. Carton, and A. D. M. Maidmentbradley, "Angular dependence of mammographic dosimeters in digital breast tomosynthesis," *Proc. SPIE* **7622**, 76225L (2010).
- <sup>45</sup> G. Xu, "An exponential growth of computational phantom research in radiation protection, imaging, and radiotherapy: A review of the fifty-year history," *Phys. Med. Biol.* **59**, R233–R302 (2014).
- <sup>46</sup> W. Bolch, C. Lee, M. Wayson, and P. Johnson, "Hybrid computational phantoms for medical dose reconstruction," *Radiat. Environ. Biophys.* **49**, 155–168 (2010).